Classification of Atherosclerotic Carotid Plaques Using Gray Level Morphological Analysis on Ultrasound images

E. Kyriacou [1,3], C.S. Pattichis [1], M.S. Pattichis [2], A. Mavrommatis[1], S. Panagiotou[1], C.I. Christodoulou [1,3], S. Kakkos [4], A. Nicolaides [1,4,5]
[1]Department of Computer Science, University of Cyprus, 75 Kallipoleos Str., P.O.Box 20578, 1678 Nicosia, Cyprus
ekyriac@ucy.ac.cy, pattichi@ucy.ac.cy, Andreas.mavrommatis@itd.bankofcyprus.com, stavrpan@cytanet.com.cy, cschr2@ucy.ac.cy, anicolai@cytanet.com.cy
[2]Department of Electrical and Computer Engineering, University of New Mexico, Albuquerque, USA
pattichis@eece.unm.edu
[3]Cyprus Institute of Neurology and Genetics, Nicosia, Cyprus
[4]Department of Vascular Surgery, Faculty of Medicine, Imperial College, University of London, London, UK
s.kakkos@imperial.ac.uk
[5]Vascular Screening and Diagnostic Centre, Nicosia, Cyprus

Abstract. The aim of this study was to investigate the usefulness of gray scale morphological analysis in the assessment of atherosclerotic carotid plagues. Ultrasound images were recorded from 137 asymptomatic and 137 symptomatic plaques (Stroke, Transient Ischaemic Attack -TIA, Amaurosis Fugax-AF). The morphological pattern spectra of gray scale images were computed and two different classifiers named the Probabilistic Neural Network (PNN) and the Support Vector Machine (SVM) were evaluated for classifying these spectra into two classes: asymptomatic or symptomatic. The highest percentage of correct classifications score was 66,8% and was achieved using the SVM classifier. This score is slightly lower than texture analysis carried out on the same data set.

1. Introduction

High-resolution ultrasound has made possible the noninvasive visualization of the carotid bifurcation and for that reason it has been extensively used in the study of arterial wall changes; these include measurement of the thickness of the intima

Please use the following format when citing this chapter:
Kyriacou, Efthyvoulos, Pattichis, Costas S., Pattichis, Marios S., Mavrommatis, Andreas, Panagiotou, Stavros, Christodoulou, Christodoulos, Kakkos, Stavros, Nicolaides, Andrew, 2006, in IFIP International Federation for Information Processing, Volume 204,Artificial Intelligence Applications and Innovations, eds. Maglogiannis, I., Karpouzis, K., Bramer, M., (Boston: Springer), pp. 737–744

media complex (IMT), estimation of the severity of stenosis due to atherosclerotic plaques and plaque characterization [1].

During the last decade, the introduction of computer aided methods and image standardization has improved the objective assessment of carotid plaque echogenicity, and heterogeneity [2], and has largely replaced subjective (visual) assessment [1], that had been criticized for its relatively poor reproducibility [3].

Previous studies investigated the usefulness of texture analysis [4-8], and more recently, multiscale morphological analysis was also used [6-9] towards the development of a Computer Aided Diagnostic (CAD) system for the classification of asymptomatic and symptomatic atherosclerotic plaques. These studies gave promising results.

Through this study we try to investigate gray scale morphological analysis in the aforementioned classification, and compare the findings with other studies.

The paper is structured as follows; section 2 describes the material, image acquisition, normalization and segmentation of plaque images. Sections 3 and 4 describe the gray scale morphological analysis and the classification algorithms, respectively. Section 5 gives the results and section 6 the concluding remarks.

2. Material, Image Acquisition, Normalization and Segmentation

A total of 274 carotid plaque ultrasound images (137 asymptomatic plaques and 137 symptomatic plaques associated with retinal or hemispheric symptoms (33 stroke, 60 TIA, and 44 AF). Patients with cardioembolic symptoms or distant symptoms (> 6 months) were excluded from the study. Asymptomatic plaques were truly asymptomatic if they had never been associated with symptoms in the past associated with retinal or hemispheric symptoms (Stroke, TIA or AF), i.e. unstable plaques.

The ultrasound images were collected in the Irvine Laboratory for Cardiovascular Investigation and Research, Saint Mary's Hospital, UK, using an ATL (model HDI 3000 - Advanced Technology Laboratories, Seattle, USA) duplex scanner with a linear broadband width 4-7 MHz (multifrequency) transducer, at approximately a resolution of 20 pixels/mm.

The images were normalized manually by adjusting the image linearly so that the median gray level value of blood was in the range of 0-5, and the median gray level of adventitia (artery wall) was in the range of 180-190 [10]. The scale of the gray level of the images ranged form 0 to 255. This normalization (i.e. using blood and adventitia as reference points) was necessary in order to extract comparable measurements in case of processing images obtained by different operators or different equipment [10].

The plaque identification and segmentation tasks are quite difficult and were carried out manually by a physician or vascular ultrasonographer who are experienced in scanning. The main difficulties are due to the fact that the plaque edges cannot be distinguished from blood based on brightness level difference, or using only texture features, or other measures. Also calcification and acoustic shadows make the problem more complex. Thus, acoustic shadows were excluded. A system for facilitating the automated segmentation of carotid plaque based on snakes is currently under development by our group [11].

3. Gray Scale Morphological Analysis

Morphological features are motivated from the need to study the basic structure of the plaque. In this study we used gray scale morphological analysis in order to identify morphological features of the plaques.

The morphological features of plaques are strongly associated with events. For example black (echolucent) plaques with white big blobs are considered to be very dangerous.

In morphological image processing, we proceed to characterize the size distributions of both the blob-components which appear white, and the hole-components which appear black. For describing these components, we consider a cross structural element ('+') that does not exhibit any directional selectivity. The size distribution measures the presence of blob components of radius proportional to the positive index of the Pattern Spectrum. Similarly, the size distribution of the presence of holes is proportional to the negative index of the Pattern Spectrum. We will next provide a mathematical description of the Pattern Spectrum.

We consider pattern spectra based on a flat '+' structural element B, made up of 5 pixels. The Pattern Spectrum is defined in terms of the Discrete Size Transform (DST). We define the DST [12-13] using the following equations:

$$f \rightarrow (d_0(f;B), d_1(f;B), \ldots d_k(f;B)) \quad \text{where}$$
$$d_k(f;B) = fokB - fo(k+1)B,$$

o denotes an open operation. The binary DST is a multi-resolution image decomposition scheme, which decomposes an image f into residual images $f \circ kB - f \circ (k+1)B$, for $k > 0$. The pattern spectrum of a binary image f, in terms of a structural element B, is given by:

$$P_{f;B}(k) = \|d_k(f;B)\| = \|fokB - fo(k+1)B\|, k \geq 0 \quad \text{where}$$
$$\|f\| = \sum_{x,y} f(x,y), \quad f(x,y) \geq 0$$

We note that in the limit, as $k \rightarrow \infty$, we have that the resulting image $f \circ kB - f \circ (k+1)B$ converges to the zero image. Also, we note that with increasing values of k, $f \circ kB$ is a subset of the original image. For $k \geq 0$, we may thus normalize the Pattern Spectrum by dividing by the norm of the original image $\|f\|$. Similarly, as $k \rightarrow \infty$. Thus, to eliminate undesired variations, all the pattern spectra were normalized.

The pattern spectra were computed for gray scale images using a structural element of range 1 to 70. The probability density function *(pdf)* and the cumulative distribution function *(cdf)* were computed for each plaque. An example of an asymptomatic and a symptomatic plaque with the corresponding *pdf*s and *cdf*s is shown in Fig. 1.

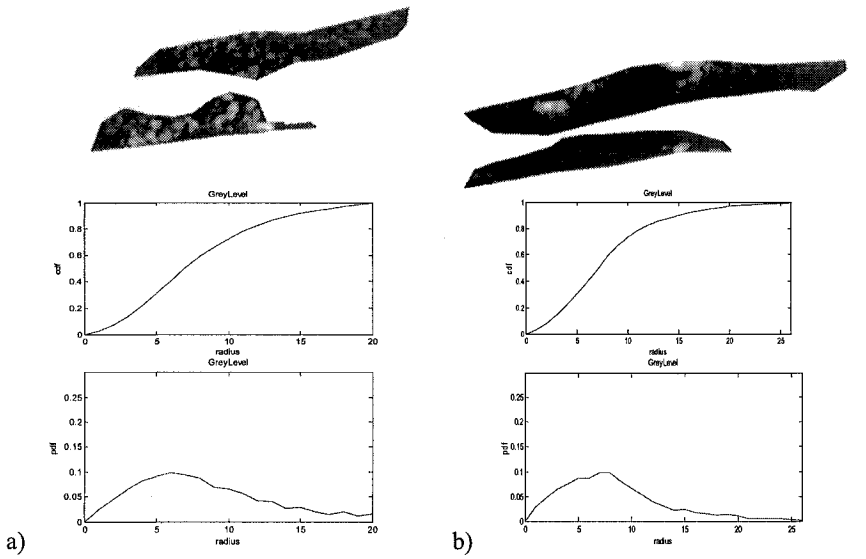

Fig. 1. a) Cumulative distribution function *(cdf)* plot and probability density function *(pdf)* for an asymptomatic carotid plaque. b) Cumulative distribution function *(cdf)* plot and probability density function *(pdf)* for a symptomatic (Stroke) carotid plaque.

4. Classification Models

The diagnostic performance of the morphological features was evaluated with two different classifiers: the Probabilistic Neural Network (PNN), and the Support Vector Machine (SVM). These classifiers were trained to classify the morphology features into two classes: i) asymptomatic plaques or ii) symptomatic plaques associated with retinal or hemispheric symptoms (Stroke, TIA or AF), i.e. unstable plaques.

The PNN [14] classifier basically is a kind of Radial Basis Function (RBF) network suitable for classification problems. This classifier was investigated for several spread radius in order to identify the best for the current problem. The SVM network was investigated using Gaussian Radial Basis Function (RBF) kernels; this was decided as the rest of the kernel functions could not achieve so good results. The SVM with RBF kernel was investigated using 10-fold cross validation in order to identify the best parameters such as spread of RBF [15].

The leave-one-out estimate was used for validating all the classification models. A total of 274 subsets of size 273 were used for training the classifiers, and the performance of the classifiers was evaluated on the remaining one subset.

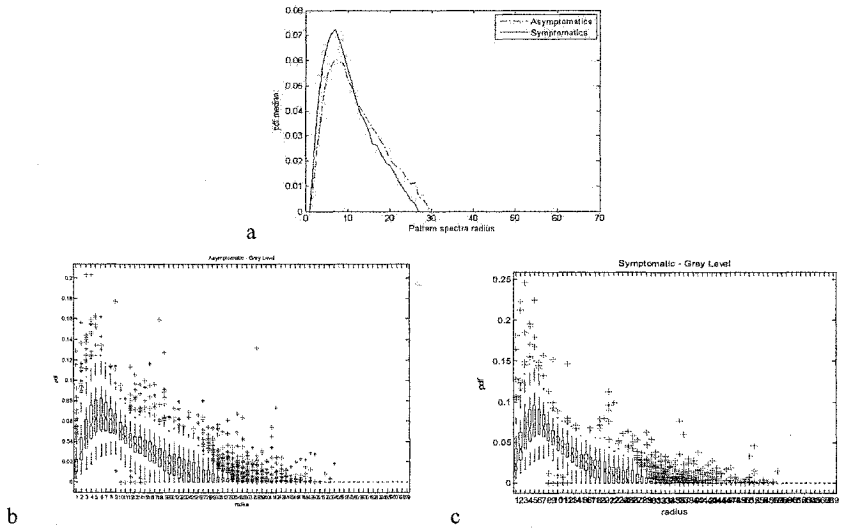

Fig. 2. a) Median probability density function *(pdf)* plots for the pattern spectra of gray scale images; symptomatic plot is plotted with a solid line while the asymptomatic one with a dotted line. b) Box plots of *pdf* for the asymptomatic carotid plaques. c) Box plots of *pdf* for the symptomatic carotid plaques. Box plots are described as follows: The notched box shows the median, lower and upper quartiles and confidence interval around the median for each feature. The dotted line connects the nearest observations within 1.5 of the inter-quartile range (IQR) of the lower and upper quartiles. Crosses (+) indicate possible outliers with values beyond the ends of the 1.5 x IQR.

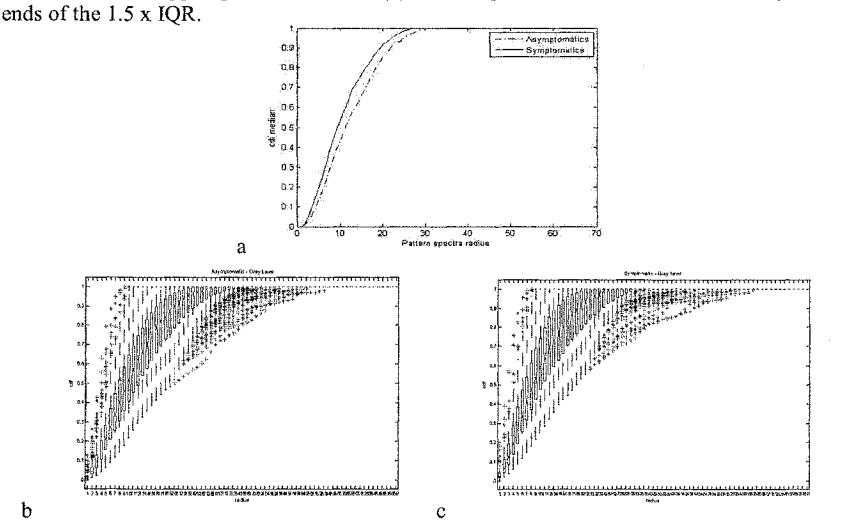

Fig. 3. a) Median cumulative distribution function *(cdf)* plots for the pattern spectra of gray scale images; symptomatic plot is plotted with a solid line while the asymptomatic one with a dotted line. b) Box plots of *cdf* for the asymptomatic carotid plaques. c) Box plots of *cdf* for the symptomatic carotid plaques.

The performance of the classifier systems were measured using the receiver operating characteristics (ROC) curves [16]. Different parameters calculated for ROC curves are true positive decision (TP) where the system classifies a plaque as symptomatic and the physician does so, false positive (FP) decision where the system does a negative diagnosis (symptomatic) and the subject is normal (asymptomatic), a false negative (FN) diagnosis where the system does a negative diagnosis (asymptomatic) and the subject is symptomatic, true negative (TN) diagnosis where the system identifies a plaque as asymptomatic and agrees with subject's condition. Sensitivity (SE) which is the likelihood that an event will be detected given it is present and Specificity (SP) which is the likelihood that the absence of an event will be detected given that is absent. Correct classification (CC) are the correct classified cases.

Table 1. Percentage of correct classifications (%CC), percentage of false positives (%FP), percentage of false negatives (%FN), percentage sensitivity (%SE) and percentage specifity (%SP) of Gray Scale morphological features using the a) PNN and b) SVM classifiers. Classification models developed for two classes using the leave one out method, and 137 symptomatic and 137 asymptomatic plaques.

SVM classifier	%CC	%FP	%FN	%SE	%SP
SVM rbf spread = 2.2627 *pdf* radii 2,3,5,10,21,23 **+PCA**	**66.79**	20.44	45.99	54.01	79.56
SVM rbf spread = 0.5657 *pdf* radii 2,3,5,10,21,23	65.33	28.47	40.88	59.12	71.53
SVM rbf spread = 2.2627 *cdf* radii 1-70 **+PCA**	63.14	42.34	31.39	68.61	57.66
SVM rbf spread = 2.2627 *cdf* radii 1-70	62.41	32.12	43.07	56.93	67.88
SVM rbf spread = 1.1314 *pdf* radii 1-70 **+PCA**	60.22	43.80	35.77	64.23	56.20
SVM rbf spread = 0.5657 *pdf* radii 1-70	**63.14**	**36.50**	**37.23**	**62.77**	**63.50**

PNN classifier	%CC	%FP	%FN	%SE	%SP
PNN spread =5 *pdf* radii 2,3,5,10,21,23 **+PCA**	56.57	22.63	64.23	35.77	77.37
PNN spread =5 *pdf* radii 2,3,5,10,21,23	56.57	22.63	64.23	35.77	77.37
PNN spread =5 *cdf* radii 1-70 **+PCA**	60.58	36.50	42.34	57.66	63.50
PNN spread =5 *cdf* radii 1-70	**62.04**	**35.77**	**40.15**	**59.85**	**64.23**
PNN spread =5 *pdf* radii 1-70 **+PCA**	58.76	42.34	40.15	59.85	57.66
PNN spread =5 *pdf* radii 1-70	60.22	48.91	30.66	69.34	51.09

5. Results

The median of the probability density function *(pdf)* extracted from the plaques can be seen in Fig. 2 while the median of the cumulative distribution function *(cdf)* can

be seen in Fig. 3. Both are plotted against the radius of the pattern spectra used which is in the range of 1 to 70. According to the results we can observe that the symptomatic *cdf* is *stochastically* larger than the asymptomatic *cdf*. This implies that dark regions in the symptomatic cases were somewhat closer together, leaving smaller holes between the dark regions [17].

The *cdf*s and *pdf*s of different pattern spectra described in section 3 were used in order to classify the two classes of images using the PNN and SVM classifiers. Both classifiers were tested on both the *pdf* and c*df* feature sets. The first set included features produced for the whole range of the radii investigated (1-70) while the second set included the pattern spectra of selected radii (2, 3, 5, 10, 21, and 23) [18]. In order to decide about the second set; the discriminatory power of the different pattern spectra radii was evaluated using the C4.5 decision trees algorithm [19]. The C4.5 was run and the pattern spectra radius with the highest discriminative score was computed. This pattern spectra was then removed and the C4.5 was run again to compute the next one discriminative feature. This procedure was carried out for 5 iterations and generated columns 2, 3, 5, 10, 21, 23. The dimensionality of the feature vectors from both sets was reduced using Principal Components Analysis (PCA) to account for 98% of the total variance.

Table 1 presents the results of the ROC analysis for the SVM and PNN classifiers for the different feature sets investigated. The highest percentage of correct classifications score was 66.7% and was achieved using the SVM classifier on the second set of data (*pdf* radii 2, 3, 5, 10, 21, and 23 + PCA). For PNN models, the highest percentage of corrects classifications score achieved was 62.04% for *cdf* radii 1-70.

6. Conclusions

Concluding, morphological features can help us understand the interrelations among different plaque intensity regions in ultrasound imaging of the carotid. In this study we have examined morphological results from gray scale images and we have found that there is significant overlap between pattern spectra coming from symptomatic and asymptomatic plaques. Most of the discriminating power was concentrated in the smaller components (with radii less than 30, as shown in Fig. 2). These results are comparable to results produced for multiscale morphological analysis of a similar dataset [5-8] as well as results produced by another group [4].

In previous work carried out by our group the highest percentage of correct classifications was 73% using texture features and the self-organising map (SOM) classifier [5]. Furthermore it was shown in [6-8] that multiscale morphological analysis features compare well with the most successful texture feature sets and provide additional information for the identification of individuals at risk of stroke. The combination of texture and morphology features slightly increased the correct classifications score [17].

Future work will include the investigation of the correct classification rate on larger and different data sets and the use of clinical factors.

Acknowledgment

This work was funded through the project Integrated System for the Evaluation of Ultrasound Imaging of the Carotid Artery (TALOS), of the Research Promotion Foundation of Cyprus.

References

1. G. Belcaro, A.N. Nicolaides, G. Laurora et al., Ultrasound morphology classification of the arterial wall and cardiovascular events in a 6-year follow-up study, *Arterioscler Thromb Vasc Biol* **16**, 851-6 (1996).
2. N. El-Barghouti, A.N. Nicolaides, T. Tegos et al., The relative effect of carotid plaque heterogeneity and echogenicity on ipsilateral cerebral infarction and symptoms of cerebrovascular disease, *Int Angiol* **15**, 300-6 (1996).
3. J.A.C Arnold, K.B. Modaresi, N. Thomas et al., Carotid plaque characterization by duplex scanning. Observer error may undermine current clinical trials, *Stroke* **30**, 61-5 (1999).
4. J.E. Wilhjelm, L.M. Gronholdt, B. Wiebe, S.K. Jespersen, L.K. Hansen, H. Sillesen, Quantitative Analysis of Ultrasound B-Mode Images of Carotid Atherosclerotic Plaque: Correlation with Visual Classification and Histological Examination, *IEEE Transactions on Medical Imaging*, **17**(6), 910-922 (1998).
5. C.I. Christodoulou, C.S. Pattichis, M. Pantziaris, A. Nicolaides, Texture Based Classification of Atherosclerotic Carotid Plaques, *IEEE Tr. on Med. Im.*, **22**, 902-912 (2003).
6. C.I Christodoulou, E. Kyriacou, M.S.Pattichis, C.S. Pattichis, A. Nicolaides, " A Comparative Study of Morphological and other Texture Features for the Characterization of Atherosclerotic Carotid Plaques", *Proc of CAIP 2003,* The Nederlands, 165-173, (2003).
7. C.I. Christodoulou, C.S. Pattichis, E. Kyriacou, M.S. Pattichis et. al., in:Applied Medical Image Analysis Methods. ed. by L. Costaridou, (CRC Press 2005), 87-135.
8. E. Kyriacou, M.S. Pattichis, C. Christodoulou, C.S. Pattichis, S. Kakkos, A. Nikolaides, in: Plaque Characterization using Multimodality Imaging: Pixel to Molecular, Ed. by J.S. Suri, C. Yuan, D.L. Wilson, S. Laxminarayan, (IOS Press, 2005), 241-275.
9. E. Kyriacou, M. Pattichis , C. Christodoulou , C. Pattichis, S. Kakkos , A. Nicolaides, Multiscale Morphological Analysis of the Atherosclerotic Carotid Plaque, *Proceedings of the 27th Annual Int. Conf. IEEE EMBS*, Shanghai, China (2005).
10. T.J. Tegos, M.M. Sametai, A.N. Nicolaides et al., Comparability of the ultrasonic tissue characteristics of carotid plaques, *J Ultrasound Med* **19**, 399-407 (2000).
11. C. Loizou, C. Pattichis, R. Istepanian, M. Pantziaris, A. Nicolaides, Atherosclerotic Carotid Plaque Segmentation, *Proceedings of the 26th Annual Int. IEEE EMBS conf.* USA, (2004).
12. E.R. Dougherty, *An Introduction to Morphological Image Processing*, (SPIE Optical Engineering Press 1992).
13. P. Maragos, Pattern spectrum and multiscale shape representation, *IEEE Trans. on Pattern Analysis and Machine Intelligence* **11**, 701 715 (1989).
14. D.F Specht, Probabilistic Neural Networks, *INNS Neural Networks* **3**(1), 109-118 (1990).
15. T. Joachims 11 in: Making large-Scale SVM Learning Practical. Advances in Kernel Methods - Support Vector Learning, B. Schölkopf and C. Burges and A. Smola (ed.) (MIT Press. 1999).
16. R.C. Ebrchart, R.W. Dobbins, *Neural Networks PC Tools A Practical Guide* (Academic Pr., 1990)
17. A. Mavrommatis, *Morphology of Carotid US Images*, MSc thesis, (Univ. of Cyprus 2006).
18. S. Panagiotou, *Classification of Plaques Using SVM Class.*, MSc thesis, (Univ. of Cyprus 2006).
19. J. Han, M. Kamber, *Data Mining: Concepts and Techniques* (Morgan Kaufmann, 2000).